



Towards ultra-high ductility TRIP-assisted multiphase steels controlled by strain gradient plasticity effects



M.K. Hatami^a, T. Pardoen^b, G. Lacroix^b, P. Berke^a, P.J. Jacques^b, T.J. Massart^{a,*}

^a Université Libre de Bruxelles (ULB), Building, Architecture & Town Planning Department (BATir) CP 194/02, Avenue F.D. Roosevelt 50, 1050 Bruxelles, Belgium

^b Institute of Mechanics, Materials and Civil Engineering, Université catholique de Louvain, 1348 Louvain-la-Neuve, Belgium

ARTICLE INFO

Article history:

Received 10 November 2015

Received in revised form

21 August 2016

Accepted 19 September 2016

Available online 21 September 2016

Keywords:

TRIP steel

Strain gradient plasticity

Size effect

Homogenization

Transformation kinetics

Ductility

ABSTRACT

TRAnsformation Induced Plasticity (TRIP) is a very effective mechanism to increase the strain hardening capacity of multiphase steels containing a fraction of metastable austenite, leading to both high strength and large uniform elongation. Excellent performances have been reached in the past 20 years, with recent renewed interest through the development of the 3rd generation of high strength steels often involving a TRIP effect. The microstructure and composition optimization is complex due to the interplay of coupled effects on the transformation kinetics and work hardening such as phase stability, size of retained austenite grains, temperature and loading path. In particular, recent studies have shown that the TRIP effect can only be quantitatively captured for realistic microstructures if strain gradient plasticity effects are taken into account, although direct experimental validation of this claim is missing. Here, an original computational averaging scheme is developed for predicting the elastoplastic response of TRIP aided multiphase steels based on a strain gradient plasticity model. The microstructure is represented by an aggregate of many elementary unit cells involving each a fraction of retained austenite with a specified stability. The model parameters, involving the transformation kinetics, are identified based on experimental tensile tests performed at different temperatures. The model is further assessed towards original experiments, involving temperature changes during deformation. A classical size independent plasticity model is shown unable to capture the TRIP effect on the mechanical response. Conversely, the strain gradient formulation properly predicts substantial variations of the strain hardening with deformation and temperature, hence of the uniform elongation in good agreement with the experiments. A parametric study is performed to get more insight on the effect of the material length scale as well as to determine optimum transformation kinetics to reach the highest possible strength-ductility balance. It is shown that the uniform elongation can potentially be increased by 50% or more, paving the way towards future microstructure engineering efforts.

© 2016 Elsevier Ltd All rights reserved.

1. Introduction

Over the last decades, the demand for steels with enhanced mechanical properties, especially high strain hardening capacity, has motivated the design and manufacturing of various types of TRIP (TRAnsformation Induced Plasticity) assisted multiphase steels, e.g. Jacques (2004). Transformation induced plasticity is indeed an efficient strategy to develop alloys

* Corresponding author.

E-mail address: thmassar@ulb.ac.be (T.J. Massart).

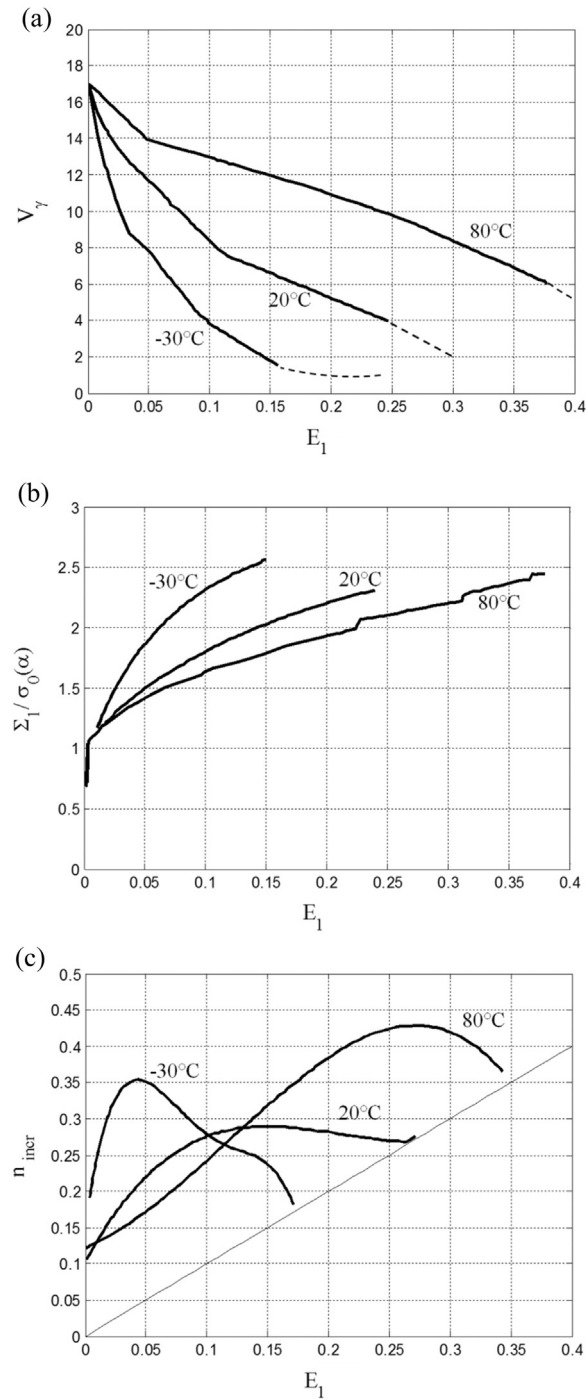


Fig. 1. Experimental results for isothermal tensile tests at different temperatures, reproduced from [Lacroix, 2007]. All quantities are plotted against the true longitudinal tensile strain (i.e. homogeneous global strain before necking): (a) kinetics of austenitic phase transformation, (b) normalized true stress-strain response (normalization is performed with respect to the initial yield of the α phase), (c) Considère plot for the determination of the onset of necking. The dashed lines represent an assumed extrapolation of the transformation kinetics beyond the experimentally detected onset of necking, as explained in Section 3.1.

with excellent strength/ductility balance. This is achieved by raising, in a controlled way, the strain hardening capacity through the continuous transformation during deformation of a fraction of metastable austenite retained owing to specific metallurgical treatments. By varying the chemical composition and the thermomechanical processing route, the volume fraction, the stability, the size and the initial strength of the retained austenite and of the surrounding ferrite-bainite matrix can be controlled. This leads to markedly different transformation kinetics and plastic behavior, see e.g. Jacques (2004);

Table 1
Chemical composition of the TRIP steel.

wt%	C	Si	Mn	P	S	Al	N
	0.31	1.51	1.57	0.009	0.008	0.009	0.004

Godet and Jacques (2015) and Jacques et al. (2007). Fig. 1 illustrates several important characteristics associated to this class of steels by showing results from an earlier investigation by Lacroix et al. (2008) and Delannay et al. (2008) with the composition reported in Table 1. Fig. 1 represents (a) the variation of the retained austenite volume fraction V_γ with deformation at different temperatures, (b) the true stress Σ/σ_0 – true strain E curves obtained for these different temperatures (σ_0 is the yield stress of ferrite), and (c) the incremental work hardening rate $n_{inc} = d \ln \Sigma / d \ln E$ with deformation. Capital letters or symbols will denote macroscopic or averaged quantities, unless stated otherwise. All quantities are reported in terms of the global, homogeneous true strain before necking. The curves presenting the variation of V_γ are extrapolated a little beyond the experimentally detected onset of necking (dashed line in Fig. 1a), for a reason that will be explained in the sequel. The strength-ductility balance strongly depends on the transformation kinetics which is controlled by the intrinsic stability of the retained austenite varying with the deformation and temperature. The temperature dependence of the hardening law of the phases is relatively small in the narrow range of temperatures considered here, and most of the difference between the responses must thus be attributed to the TRIP mechanism as observed in many earlier works on the topic, e.g. Hecker et al. (1982); Olson and Azrin (1978). The results of Fig. 1 show that the mechanical response is sensitive to the transformation of some amount of retained austenite (here typically around 15% while not completely transforming) and on the transformation kinetics. This shows the huge potential of the TRIP mechanism but also the complexity of optimizing these materials with respect to forming operations and to the final performances. In addition, it must be noted that the transformation kinetics very much depends on the loading conditions through the effect of the hydrostatic stress component on the mechanical driving force, e.g. Stringfellow et al. (1992); Lani et al. (2007) and Jacques et al. (2001).

A large number of contributions can be found in the literature dealing with the TRIP effect in steels, and a comprehensive review of this field is out of the scope of this introduction. Earlier modeling works have been devoted to various classes of TRIP steels, such as single phase austenitic steels, e.g. Hecker et al. (1982), or multiphase steels, Jacques et al. (2001). A short review of the modeling strategies is provided here. These approaches are classified based on the considered scale, irrespective of the family of TRIP steel. In order to model TRIP effects, different deformation mechanisms active at the fine scale should be considered, see Cherkaoui et al. (1998). Their interactions with microstructural evolutions, along with energetic considerations, control the orientation and accommodation effects, denoted as the Magee (1970) and Greenwood-Johnson (1965) effects, respectively.

Olson and Cohen (1975) developed a seminal model linking the evolution of the martensite volume fraction to the accumulated plastic strain, with shear band intersections as the most probable zone to accommodate strain-induced transformation. This model was later extended by Stringfellow et al. (1992), using the mechanical driving force in a two-phase composite material, to incorporate the hardening effects, induced by the presence of the martensitic phase, as well as the effect of the hydrostatic stress component. Tomita and Iwamoto (1995) further developed the Stringfellow model by including strain rate effects.

Other models involved a finer scale description of the material. In the model proposed by Marketz and Fischer (1994), crystallographic and thermodynamic aspects of the martensitic transformation are coupled in order to investigate both the Magee and Greenwood-Johnson effects. Cherkaoui et al. (1998) developed a thermo-micromechanical model to represent such effects, including an inelastic strain within the martensitic phase for the phase transformation. A model based on internal variables was introduced by Fischer et al. (1998) to account for plastic flow and the progress of the transformation. Idesman et al. (1999) derived a model in a finite strain setting, in which the potential region undergoing transformation is imposed, and in which the final phase configuration is assumed in the model as from the start of the calculation.

Multi-scale approaches were developed to link the micro and macro scales characteristics. Levitas et al. (1998) showed that the geometry of the transformation is controlled by the maximum transformation work, a condition satisfied near the shear band intersections. Diani et al. (1995) focused on the relationship between the macroscopic and the microscopic strain fields in TRIP steels. Marketz and Fischer (1995) extended their former micromechanical model to mesoscale aspects by incorporating the effect of micro-stresses. In Kouznetsova and Geers (2007), a multiscale approach was developed in which the effect of plastic deformation of the parent phase on the product phase is incorporated. Leblond et al. (1986) developed a model in which the evolution of the volume fraction of the martensite phase is calculated using an homogenization principle, independently from any initial assumption on the macroscopic plastic flow. Similarly, in Bhattacharyya and Weng (1994), the transformation was analyzed based on a thermo-mechanical approach without assuming a priori the martensite volume fraction evolution pattern and the plastic flow. Recently, based on the transformation criterion formulated by Fischer et al. (1998); Turteltaub and Suiker (2006a) developed a model in which the transformation driving force is incorporated in a crystal plasticity framework. The authors further developed this model to account for grain size effects (Turteltaub and Suiker, 2006b). A multiscale composite-based model for TRIP steels was also presented by Delannay et al. (2008), in which the evolution of the martensitic phase is controlled using the energy balance criterion proposed by Fischer et al. (1998), and in which a mean-field Mori-Tanaka approach is exploited to estimate the overall response. Recently, Srivastava et al. (2015) used large 3D FE Representative Volume

Elements (RVE) and a crystal plasticity formulation to simulate the response of TRIP assisted multiphase steels, relying on micropillar compression data for parameter identification.

Size dependency in the elastoplastic response in TRIP steels has been considered by [Turteltaub and Suiker \(2006b\)](#); [Mazzoni-Leduc et al. \(2008\)](#) and [Mazzoni-Leduc et al. \(2010\)](#), showing that strain gradient plasticity effects associated to the phase transformation can have a first order effect on the overall mechanical response. Hardening size effects were shown to be captured by higher order models in relation with evolving interface properties ([Massart and Pardoën, 2010](#); [Pardoën and Massart, 2012](#)). The reason for the size dependency in the TRIP effect is that transformation involves austenite regions which are in the range of 1 μm and which, upon transformation, lead to strong plastic strain gradients in the close neighborhood. [Mazzoni-Leduc et al. \(2008, 2010\)](#) used the strain gradient plasticity model developed by [Fleck and Hutchinson \(2001\)](#), to investigate the effects of transformation on the material behavior of TRIP steels. Although this model revealed strong effects of the plastic strain gradients on the impact of the TRIP mechanism on the response of unit cells made of a single transforming grain, no direct or even indirect comparison with experimental results could be made.

Based on this current state of literature, the present work addresses several new or open aspects. The first goal is to prove that a size dependent (strain gradient) based plasticity formulation is required to capture the significant effect of the transformation kinetics on the strain hardening and on the strain at necking by direct comparisons with experiments while classical plasticity fails at doing so. Secondly, a relatively original homogenization scheme is built up to describe the evolving multiphase microstructure. Thirdly, a finite strain version of the SGP theory has been implemented in order to deal with strength and ductility evolution at large deformation (while our earlier work used a small strain version). Fourthly, original experimental results involving tensile tests with sharp temperature changes and the corresponding evolution of the martensitic phase transformation are also addressed to further exploit the model. Finally, new perspectives are proposed towards the future optimization of TRIP steels by tuning the transformation kinetics.

To achieve these objectives, the unit cell model developed by [Mazzoni-Leduc et al. \(2008, 2010\)](#) is extended by addressing representative volume elements that are rich enough to encompass a large number of austenite grains, each one transforming at a different level of deformation. For this purpose, an averaging procedure is set, similar in spirit to the one used by [Ognedal et al. \(2014\)](#). The constitutive model of the material is based on the strain gradient plasticity formulation of [Fleck and Hutchinson](#) in a 2D finite deformation setting as developed by [Niordson and Redanz \(2004\)](#). The model parameters are first identified in order to reproduce the trends presented in [Fig. 1](#) followed by a validation using data obtained with the same TRIP steels but with temperature changes during deformation. Finally, a parametric study is performed to get more insight on the effect of the material length scale, as well as to determine the optimum transformation kinetics to reach the highest possible strength ductility balance. This last analysis is also motivated by the major recent interest for the development of the so-called “third generation” of high strength steels. Such steels are based on multiphase extremely fine martensitic/bainitic microstructures for the strength, with moderate amount of alloying elements often designed to combine both TWIP (Twinning Induced Plasticity) and TRIP effects, owing to the presence of small layers of austenite. The remarkable properties demonstrated in the very recent literature, e.g. [Wang et al. \(2014\)](#); [Raabe et al. \(2009\)](#) and [Wang et al. \(2014\)](#) are indeed partly related to a TRIP effect associated to extremely fine austenite regions for which the present model is particularly relevant at least to deal with the first order effects, see also recent work by [Yen et al. \(2015\)](#).

The outline of the paper is the following. [Section 2](#) describes the unit cell model, the transformation and constitutive models, recalling the essentials of the strain gradient plasticity formulation. The homogenization scheme used to impose the transformation kinetics and to aggregate the results of the single cells in order to predict the overall behavior is explained in [Section 3](#). The connection between the experimentally inspired transformation kinetics and the loading conditions applied on unit cells are also presented, as well as the global averaging procedure used to generate the macroscopic response based on a discretized kinetics of the transformation. [Sections 4–6](#) present the numerical results obtained using this approach together with a discussion and the comparison with the experimental data reported by [Lacroix \(2007\)](#) for isothermal tension, as well as the non-isothermal tensile tests. Finally, [Section 7](#) concludes with future perspectives.

2. Model and numerical procedures

2.1. Description of the representative volume element

As a fully realistic microstructure representation would be too complex to use in the present approach, a simplified 2D unit cell is used to model the TRIP assisted multiphase steel, see [Fig. 2](#). This configuration was used by [Mazzoni-Leduc et al. \(2008, 2010\)](#) to study the TRIP mechanism effects at the scale of a single transforming grain using the Fleck-Hutchinson strain gradient plasticity formulation. A circular austenitic inclusion surrounded by a ferritic matrix partially transforms into a martensitic phase as a result of mechanical loading. The key features of the microstructure that are taken into account are (i) the (evolving) volume fractions of austenite and of martensite and (ii) the orientation of the newly formed martensitic inclusion chosen to maximize the mechanical driving force for transformation. In case of uniaxial tensile loading, the potential zone to be transformed is aligned at 45° with respect to the tensile loading direction, see [Van Rompaey et al. \(2006\)](#). Furthermore, an elliptical shape is chosen in order to prevent stress singularities at the tips of the transformed area, which would artificially increase the effect of strain gradients.

The geometry described above is sketched in [Fig. 2](#) with the configurations before, during, and after phase

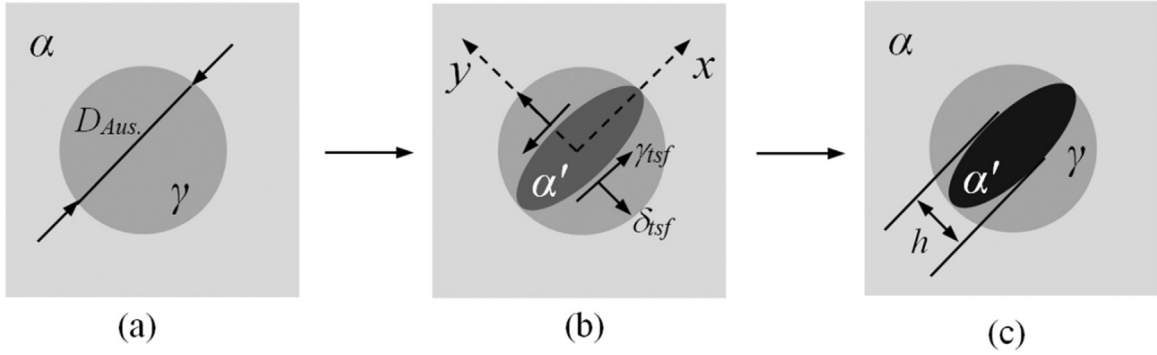


Fig. 2. Microstructural unit cell model for the phase transformation process: (a) before transformation, (b) during transformation and (c) after transformation. The transformation strain or eigenstrain – denoted with components δ_{tsf} and γ_{tsf} in the local axis frame (see relation (2)) – is applied on the transforming zone through step (b). The parameters of the transformation strain will be taken as $\delta_{tsf} = 0.03$ and $\gamma_{tsf} = 0.1$ in the sequel. (α : ferrite, γ : austenite and α' : martensite).

transformation. All the steps used in order to model the phase transformation will be explained next. In this work, classical notations used in the metallurgical terminology are used to refer to different phases: α for ferrite, γ for austenite and α' for martensite. Based on experimental data that will be used for the assessment of the model, see Lacroix (2007), the volume fraction of the residual austenite inclusion is set to 17%, with an assumed (simplified) circular shape, as depicted in Fig. 2. The potential elliptical martensite phase, with a size set by the austenitic inclusion size, is surrounded by the austenite inclusion. The size and thus the volume fraction of the martensitic inclusion is controlled by the dimension h of its minor axis, see Fig. 2.

2.2. Phase transformation model and numerical treatment

In the present study, the martensite formation and evolution is explicitly prescribed. Hence, we focus only on the evolving composite effect resulting from the TRIP effect (which involves also the change of hardening behavior of the transforming region) assuming the transformation kinetics is incorporated exactly. In the present study, Σ_{cell} and E_{cell} always refer to the overall macroscopic true stress and strain averaged over the unit cell, respectively, unless otherwise stated. They are computed as follows

$$\begin{aligned}\Sigma_{cell} &= \frac{1}{V_{cell}} \int_{V_{cell}} \sigma \, dV_{cell}, \\ E_{cell} &= \frac{1}{V_{cell}} \int_{V_{cell}} \varepsilon \, dV_{cell}.\end{aligned}\quad (1)$$

In the sequel, the subscript 'cell' will be omitted for brevity whenever possible. In the present approach, we will assume that the transformation strain is applied instantaneously with respect to the overall (macroscopic) mechanical loading. Assuming thus a homogeneous progress in the mechanical effect of the material transformation, the transformation is simulated locally using the following three successive stages:

1. The material is subjected to the tensile loading conditions until a specific overall average unit cell true strain level $E_{tsf}^{init,cell}$ is reached. The material is assumed to be composed of ferrite and austenite only as shown in Fig. 2a, i.e. $E = \langle E \rangle_{\alpha+\gamma}$. The computation of $E_{tsf}^{init,cell}$ based on experimental macroscopic strain data will be explained in detail later.
2. When the average strain in the unit cell E_{cell} reaches the threshold value $E_{tsf}^{init,cell}$, the material properties of the elliptical zone are gradually updated from the austenite to the martensite properties. Simultaneously, the macroscopic, overall mechanical loading is temporarily stopped (the loading of the cell will be applied through a surrounding medium, as explained in Section 2.5) and a transformation eigenstrain is imposed to the appearing martensitic phase. The eigenstrain is associated to the transformation itself, i.e. it is the strain that the transforming region would undergo if it would freely deform. Since this eigenstrain occurs in a transforming region surrounded and confined by the non-transforming part of the austenite and the ferritic matrix, it will induce local stresses and plastic strain gradients. This transformation strain involves a shear γ_{tsf} as well as a dilatation δ_{tsf} component along the local axes associated with the transforming region in the representative geometry; see Fig. 2b. The martensitic phase appears instantaneously at this step (in terms of the macroscopic mechanical loading), and the transformation eigenstrain is prescribed only to this zone of the material according to the following tensor expressed in the local axes aligned with the elliptical zone

$$\varepsilon_{tsf}^{loc} = \begin{bmatrix} 0 & \gamma_{tsf}/2 \\ \gamma_{tsf}/2 & \delta_{tsf} \end{bmatrix}.\quad (2)$$

In the case of a higher order (gradient plasticity) formulation, a plastic confinement condition should be applied along the freshly nucleated martensitic phase as from this stage, to model the fact that the newly created phase boundary is impenetrable to dislocations.

3. After having applied the complete transformation eigenstrain, the transforming zone now behaves according to the martensitic elastoplastic properties, and the mechanical loading is resumed up to the selected final deformation.

2.3. Size dependent plastic constitutive model

As mentioned in Section 1, a gradient plasticity theory has been developed by Fleck et al. (1994) and reformulated by Fleck and Hutchinson (2001) to incorporate only the gradients of the plastic strain. This theory and its extended versions have been used to address many boundary value problems e.g. Niordson and Hutchinson (2003); Massart and Pardoan (2010); Legarth and Niordson (2010) and Brugger et al. (2010). Here, the theory based on only one length parameter is considered. In this formulation, the definition of the effective plastic strain increment is generalized with respect to the classical plasticity description, incorporating the gradients of the plastic strain under the form:

$$\dot{E}_p^2 = \dot{\varepsilon}_p^2 + l_*^2 \dot{\varepsilon}_{p,i} \dot{\varepsilon}_{p,i} \quad (3)$$

$$\dot{\varepsilon}_p = \sqrt{\frac{2}{3} \dot{\varepsilon}_{ij}^p \dot{\varepsilon}_{ij}^p}$$

where \dot{E}_p is the rate of the generalized plastic strain, $\dot{\varepsilon}^p$ and $\dot{\varepsilon}_{p,i}$ are the conventional effective plastic strain rate and its spatial gradients, respectively, while $\dot{\varepsilon}_{ij}^p$ are the components of the plastic strain-rate tensor. In this definition, l_* denotes a material internal length parameter that sets the scale at which the effects of the plastic gradients become dominant. Basically, it has been argued that the first part of the generalized effective plastic strain corresponds to effects due to the statistically stored dislocations (SSDs), while the second part arises from the presence of geometrically necessary dislocations (GNDs) (Evans and Hutchinson, 2009). Due to the path-dependency and the strongly non-proportional local loading conditions in the microstructure when TRIP effects are modeled, the incremental form of the formulation proposed by Fleck and Hutchinson (2001) will be used here. This formulation is briefly summarized for completeness.

According to Fleck and Hutchinson (2001), the classical J_2 flow theory is generalized such that the principle of virtual work incorporates a stress measure (Q) and higher order stresses (τ_i) conjugate to the generalized plastic strain and to the plastic strain gradients, respectively. The principle of virtual work can be expressed in the current configuration for large strain problems according to Niordson and Redanz (2004) as follows:

$$\forall \delta \dot{u}_i \text{ and } \forall \delta \dot{\varepsilon}_p: \int_V (\sigma_{ij} \delta \dot{\varepsilon}_{ij} + (Q - \sigma_{(e)}) \delta \dot{\varepsilon}_p + \tau_i \delta \dot{\varepsilon}_{p,i}) dV = \int_S (T_i \delta \dot{u}_i + t \delta \dot{\varepsilon}_p) dS \quad (4)$$

where σ_{ij} and $\sigma_{(e)}$ are the Cauchy stress tensor and the corresponding equivalent von Mises stress, respectively. Q is the generalized effective stress, work conjugate to the plastic strain ε_p , while τ_i is the higher order stress conjugate to the gradient of the effective plastic strain.

T_i is the classical traction acting at the continuum boundary while t is the higher-order traction at the boundary of the plastically deforming part of the body. V and S serve as the domain volume and surface, respectively. In the absence of body forces and using the Gauss theorem, the strong form of equilibrium, the consistency equation, incorporating higher order effects as well as the higher-order boundary conditions can be recovered from Eq. (4), as extensively developed by Fleck and Hutchinson (2001).

This leads to the equilibrium equation

$$\dot{\sigma}_{ij,j} = 0, \quad (5)$$

and to the generalized field consistency equation

$$\dot{\sigma}_{(e)} = \dot{Q} - \dot{\tau}_{i,i} \quad (6)$$

that defines the generalized effective stress.

In order to rewrite the principle of virtual work in the reference configuration, one can define the Kirchhoff stress measures for each stress quantity defined above from the true and higher-order stress measures as:

$$\zeta_{ij} = J \sigma_{ij}, \quad \sigma_{(e)}^{\zeta} = J \sigma_{(e)}, \quad q = JQ, \quad \rho_i = J \tau_i \quad (7)$$

where J is the determinant of the deformation gradient tensor. As a consequence of applying the updated Lagrangian scheme to Eq. (4), the reference frame is taken identical to the current frame ($J = 1$). To ensure objectivity of the stress measures, Jaumann and convected rates of the Kirchhoff stress and the higher-order stress measures are employed, respectively, see Niordson and Redanz (2004). By straightforward manipulations, the incremental expression of the principle of virtual work can be reformulated in the following form:

$$\int_V \left(\overset{\nabla}{\zeta}_{ij} \delta \dot{\epsilon}_{ij} - \sigma_{ij} (2 \dot{\epsilon}_{ik} \delta \dot{\epsilon}_{kj} - \dot{\epsilon}_{kj} \delta \dot{\epsilon}_{ki}) + (\dot{q} - \sigma_{(e)}^{\zeta}) \delta \dot{\epsilon}_p + \dot{\rho}_i \delta \dot{\epsilon}_{p0,i} \right) dV = \int_S (\dot{T}_{0i} \delta \dot{u}_i + \dot{t}_0 \delta \dot{\epsilon}_p) dS \quad (8)$$

where the subscript ‘0’ stands for the reference coordinate system and $\dot{\epsilon}_{ij}$ is the rate of the velocity gradient ($\nabla \dot{u}$). Moreover, the Jaumann ($\overset{\nabla}{\cdot}$) and convected ($\overset{\circ}{\cdot}$) rates of the corresponding stress measures are defined as

$$\overset{\nabla}{\zeta}_{ij} = \dot{\zeta}_{ij} - \dot{\omega}_{ik} \sigma_{kj} - \sigma_{ik} \dot{\omega}_{jk}, \quad (9)$$

$$\dot{\rho}_i = \dot{\rho}_i - \dot{\epsilon}_{ik} \rho_k. \quad (10)$$

The reason for choosing the convected rate of the higher-order stress is to benefit from the symmetry of stiffness matrix in solving the discretized version of Eq. (4) (Niordson and Redanz, 2004). In Eq. (9) ω_{ij} denotes the skew-symmetric part of the velocity-gradient tensor which defined in an incremental form as

$$\dot{\omega}_{ij} = \frac{1}{2} (\dot{\epsilon}_{ij} - \dot{\epsilon}_{ji}). \quad (11)$$

The constitutive equations used to update the stress measures in the finite strain framework are expressed as a function of the total generalized plastic strain, the plastic strain rate and its spatial gradients according to Eqs. (12)–(14):

$$\overset{\nabla}{\zeta}_{ij} = L_{ijkl} (\dot{\epsilon}_{kl} - \dot{\epsilon}_p m_{kl}) \quad (12)$$

$$\dot{q} = h(E_p) \dot{\epsilon}_p \quad (13)$$

$$\dot{\rho}_i = l_{*}^2 h(E_p) \dot{\epsilon}_{p,i} \quad (14)$$

where L_{ijkl} refers to the elastic stiffness tensor for an isotropic material, where the plastic tangent modulus h is the derivative of the hardening law with respect to the plastic strain ($\partial \sigma_y(E_p) \partial / E_p$), representing the effect of the accumulation of dislocations, and where m_{kl} represents the direction of the plastic strain tensor. One of the key element of the Fleck and Hutchinson theory is to evaluate both the hardening and its derivative at E_p (as the hardening parameter) instead of at ϵ_p in the classical plasticity theory, to account for the effect of both geometrically necessary and statistically stored dislocations on the hardening response.

2.4. Numerical implementation of the SGP model

A 2D plane stress finite element formulation of the model has been implemented for the purpose of the present study. 6-noded triangular elements are used. The variations of the displacement and of the effective plastic strain fields are interpolated through quadratic and linear shape functions respectively, with displacement degrees of freedom defined at all nodes, and effective plastic strain degrees of freedom defined at corner nodes of the elements. The incremental principle of virtual work is used within an explicit procedure; small time steps are therefore used for the loading discretization to avoid major deviations from equilibrium. The resulting set of discretized equations is straightforwardly obtained by substitution of the approximation in the incremental principle of virtual work, see Niordson and Redanz (2004). The presence of the plastic strain increments as unknowns of the set of discretized equations requires the prescription of higher-order boundary conditions at the plastic boundary of the continuum. These specific boundary conditions, to be applied at material interfaces as a function of their response to dislocation glide, are classified in Fig. 3 together with their expression and mechanical interpretation.

The higher-order boundary conditions, applied at external boundaries, are dependent on the problem configuration. At a surface where dislocations can flow unimpeded, no restriction is set on the plastic strain. Likewise, the evolving elastic-plastic boundary within a given phase of the continuum will here be kept ‘plastically unconstrained’ as proposed by Mazzoni-Leduc et al. (2008). Note that at internal boundaries within a microstructure involving a continuously appearing hard phase, the plastic flow should be assumed to vanish along the boundary of this phase upon transformation. In this strain gradient plasticity formulation, the consistency condition is expressed using the generalized effective stress measure (Q), instead of the classical von Mises stress in classical plasticity defined in the hardening model ($\sigma_{(e)}$). Within the incremental procedure, an elastic unloading is considered upon appearance of a negative value for the plastic strain increments delivered by the discretized system of equations.

A mesh consisting of more than 12,000 elements and 42,000 nodes generated with the open source software GMSH (Geuzaine and Remacle, 2009) is used for the discretization of the model in the computations reported in the sequel.

2.5. Higher order boundary conditions and overall loading

As described in Sections 2.3–2.4, the plastic strain unknowns can be explicitly prescribed in a gradient plasticity formulation. This key feature is useful to study size effects in an evolving TRIP microstructure since the interface between the

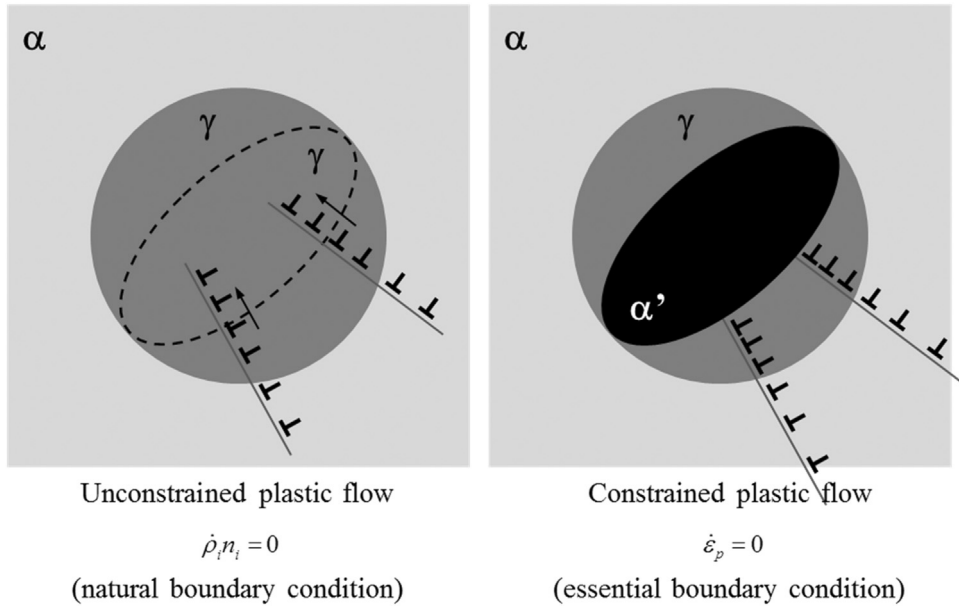


Fig. 3. Higher order boundary conditions associated with the strain gradient plasticity formulation: (left) austenitic inclusion with no interface impeding dislocation glide, (right) hard martensitic inclusion boundary preventing dislocation glide, leading to dislocation pile-ups.

austenite and the martensite phases act as a boundary impenetrable to dislocation. Hence, before transformation, there is no constraint imposed inside the austenite grain while the plastic flow gets constrained along the elliptical martensite boundary ($\dot{\epsilon}_p = 0$) as from the start of the phase transformation. Note that the moving elasto-plastic boundary within a given phase is not constrained here, see [Niordson and Hutchinson \(2003\)](#) for more details. The values defining the magnitude of the local transformation strain are kept constant for all cases.

Applying a stress-free transformation with prescribed loading conditions applied directly through the unit cell boundary delivers two bounds of the average response: traction-controlled boundary conditions on the unit cell would keep the overall stress, denoted as $\Sigma_{tsf}^{init,cell}$, constant during the application of the transformation eigenstrain in stage 2 defined in [Section 2.2](#). Conversely, the displacement-controlled boundary conditions would have similar effects, maintaining the cell average strain constant during the transformation, see [Mazzoni-Leduc et al. \(2008\)](#). In reality, the phase transformation does not occur at constant levels of stress or strain locally. In order to avoid such a non-physical effect of the unit cell mechanical control on the obtained average material response, the unit cell is embedded in a surrounding medium as suggested in the literature, see [Van Rompaey et al. \(2006\)](#). The presence of this surrounding medium allows controlling the overall macroscopic strain through a far field quantity E_{far} . This surrounding medium is given material properties equivalent to the initial composite made of a ferritic matrix with austenitic inclusions. This choice of surrounding properties was made here for simplicity. For unit cells transforming at large strain levels (i.e. 'late'), this introduces an approximation. Such cells are actually surrounded by a medium closer to the average TRIP response that has to be deduced computationally. Constant properties for the medium surrounding unit cells will however be used for the present approach, consistent with the simplifying assumptions of the averaging scheme described in [Section 3](#). This choice will be further discussed in the results sections. The size of the surrounding composite material region is chosen such that the material response of the unit cell is independent of the selected size. In [Fig. 4](#), the subscript "cell" refers to the quantities associated with the unit cell, while "far" denotes the quantities applied along the boundaries of the entire model, including the surrounding composite. The value of the aspect ratio $\frac{L_{cell}}{V}$ was chosen larger than $\frac{1}{5}$, see ([Dong and Schmauder, 1996](#)). In order to represent a tensile loading, the complete model is subjected to a uniform horizontal displacement U_{far} . The transformation within the unit cell now occurs under constant U_{far} (or E_{far}), i.e. only the far field boundary is temporarily fixed during the eigenstrain transformation, which means that no a priori assumption is made on the evolution of Σ_{cell} or E_{cell} during the transformation. Knowing the properties of the surrounding medium, a direct link can be determined between the far field applied strain, and the corresponding average strain in the unit cell.

In practice, a fictitious generalized thermal strain is applied to the martensite region in order to represent the transformation strain using Eq. (2). The components of the transformation strain (containing off-diagonal terms unlike 'classical' thermal strains) are parametrized using an artificial dependency to a field uncoupled from the displacement field (similar to the application of a 'classical' temperature field). All the components of the transformation strain are proportionally increased by imposing an artificial temperature field inside the transforming martensitic region only.

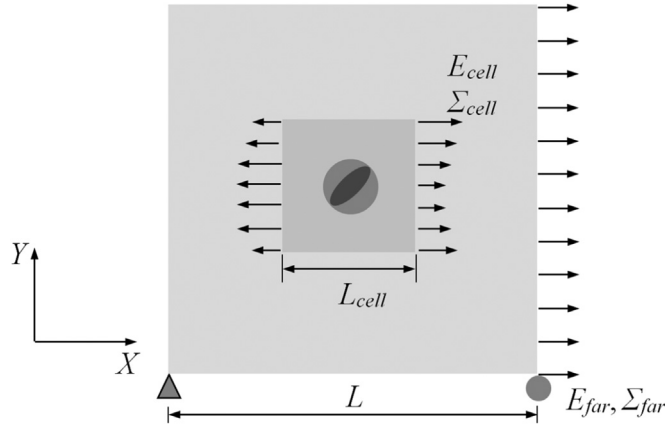


Fig. 4. Embedded cell model for applying the far field loading to the embedded unit cell.

2.6. Typical single unit cell response

The typical responses of the unit cells is depicted in Fig. 5, in which each curve represents the response of a single cell which has its specific level of strain at the start of the martensitic transformation. The methodology for recombining these curves in order to compute the overall response will be explained in Section 3. As can be noted, the effect of the eigenstrain is visible in the curves: upon the start of the transformation, the eigenstrain dilatation induces a drop in the average stress level. This stress drop is followed by an increase of the stress level when the martensitic region is fully formed and the application of the eigenstrain is completed. Conforming with the description in Section 2.5, this subsequent stress increase is significantly affected by the development of strong plastic strain gradients. These gradients result from the combined effect of the accommodation of the transformation strain and of the new higher order plastic conditions $\dot{\epsilon}_p = 0$ at the impenetrable interphase. To illustrate this, the local distribution of effective plastic strain corresponding to three levels of deformation of a transforming unit cell are given in Fig. 5. These plastic strain distributions correspond to the unit cell responses depicted in bold in Fig. 5, and to the master set of material parameters used in the sequel of the paper.

3. Homogenization procedure

This section describes the methodology used for combining the results obtained from different unit cells representing different local material behaviors in order to capture the global response of the TRIP steel with an heterogeneous transformation kinetics. The fact that some γ islands transform at larger strains than others, can be due to several factors such as the dispersion in carbon content and the local environment (i.e. variations of the shape of the austenite islands, the presence of bainite next to the austenite, the orientation of the grain; which all affect the stress transfer in the austenite grain while not being taken into account in the simplified description of the elementary unit cell). The martensitic transformation process involves nucleation and growth of martensite variants within retained austenite grains. However, the key physical point here is that one variant of α' transforms very fast (which is what is simulated with the approach explained in Section 2.2) and not progressively with respect to the overall macroscopic loading, but that different austenite grains transform at different deformation levels.

The main focus is first set on the development of a numerical technique able to capture the experimental trends for the TRIP steels and the various transformation kinetics reported by Lacroix (2007) in order to assess its potential or validity. However, the method is not restricted to this case and can be extended for other types of TRIP steels or transforming materials as well as to perform parametric studies such as the one proposed at the end of the paper. This “homogenization” approach is inspired from the work by Ognedal et al. (2014), originally defined in a different context to simulate heterogeneous damage evolution. Since the phase transformation occurs locally in the course of deformation, the overall material is assumed to be divided into several unit cells, assuming that each of them can be simulated independently from the others, i.e. no effect of neighboring transforming inclusions on the kinetics of the local transformation of a given inclusion is taken into account. This allows initiating the transformation process at different unit cell average strain levels for different unit cells. The stepwise description of the procedure is presented hereafter.

3.1. Averaging of experimentally determined transformation kinetics

The experimental transformation kinetics is employed to identify the distribution of macroscopic strain levels at which the transformation initiates. A polynomial fitting is used to represent the experimental variation of V_γ with the macroscopic

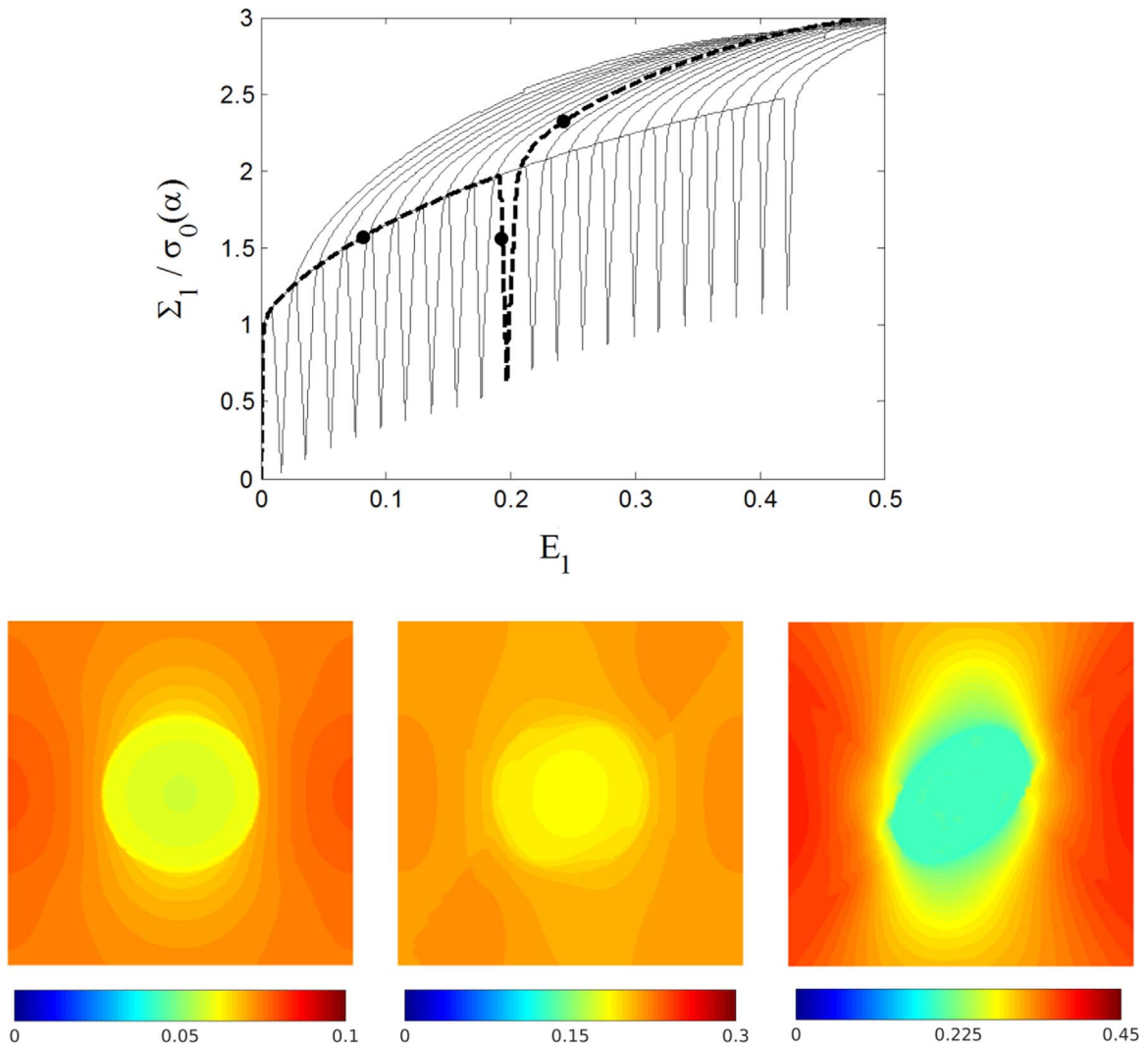


Fig. 5. Unit cell responses and local plastic strain gradients development as a result of the transformation strain. The color bar is adapted to the plastic strain levels present in each of the deformed state of the cell. (Top) set of unit cell averaged true stress – true strain responses, (bottom) plastic strain distribution corresponding to three stages of deformation during the unit cell computation corresponding to the bold curve (markers on the curve denote the states at which plastic strains are plotted in the contour plots). (For interpretation of the references to color in this figure legend, the reader is referred to the web version of this article.)

strain E_{cell} . Accordingly, the initiation unit cell strain values corresponding to the transformation of each of the successive volume fractions (e.g. $E_{tsf1}^{init,cell}$ for $V_{\gamma 1}$ and $E_{tsf2}^{init,cell}$ for $V_{\gamma 2}$ see Fig. 6) can be calculated. The variation of V_{γ} is “discretized”, and for each discretized interval, the mean value of the strain levels is recorded as the value at which the transformation initiates for a given unit cell (E_m^{cell} in Fig. 6). In practice, the transformation kinetics domain is completely discretized using this approach, thereby providing the set of macroscopic strain levels at which transformation starts. Each of these strain levels indicates the value at which transformation occurs in a unit cell that represents the collective effect of the local responses of all the austenitic grains transforming during that strain interval. All the unit cells are computed independently (without exchange of information), and the transformation strain occurs with an evolution of the average strain in the cell. As already mentioned, the unit cell is surrounded by a medium with material properties that correspond to the average behavior of a non-transforming cell. The effect of this assumption is discussed in the sequel. For a given transformation kinetics, a set of unit cells thus predicts the local behavior for different starts of transformation.¹ Here, the variation of V_{γ} presented by Lacroix (2007) or Delannay et al. (2008) is considered. Isothermal tests for the temperatures -30°C , 20°C and 80°C (Lacroix, 2007)

¹ The set of strain levels selected to initiate the transformation in the different cells, corresponds to the macroscopic unit cell strain and not to the far field strain.

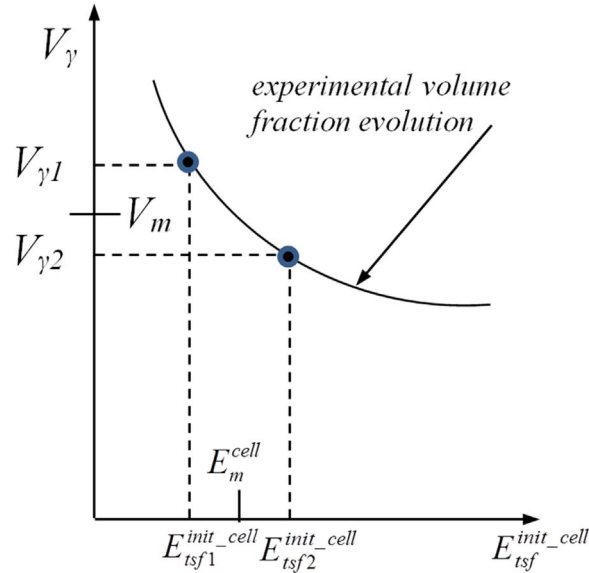


Fig. 6. Discretization of the deformation domain with respect to the transformation kinetics to identify the set of strain at which the transformation is activated in each unit cell.

are considered first, while two complementary non-isothermal transformation tests, with temperature variations $-30\text{ }^{\circ}\text{C}/20\text{ }^{\circ}\text{C}$ and $80\text{ }^{\circ}\text{C}/20\text{ }^{\circ}\text{C}$, are addressed next. The experimental V_γ evolution is reported until detection of the onset of necking. The experimental kinetics are extrapolated by a few percent beyond the point of deformation at which necking is detected experimentally (indicated by a dashed line in Fig. 1(a)). This allows computing unit cell responses beyond this deformation level, thereby avoiding introducing any a priori knowledge of the experimental necking detection in the input data of the simulation and in the averaging scheme. The total number of unit cells varies from case to case, between 18 and 30. This fitting of the experimental transformation kinetics could obviously be replaced by a physical transformation model such as proposed by Fischer et al. (1998), which is left for future works. Here, the idea is to validate the constitutive model and the homogenization scheme alone independently of the additional approximations and errors that would be associated to a phase transformation model.

3.2. Control of the loading and transformation

Since the loading conditions are actually imposed through the far field at the external boundary of the model, see Fig. 4, it is necessary to connect the unit cell macroscopic true strain at which transformation starts ($E_{tsf}^{init,cell}$ set by the experimentally observed kinetics) to the far field nominal strain (E_{far}^{nom}). To this end, the tensile response of the complete model (cell + surrounding) without phase transformation is determined; see Fig. 7a. Based on the result of this simulation, the unit cell averaged true strain can be computed from relationship (1) for all E_{far}^{nom} levels, and the link between E_{far}^{nom} and an embedded unit cell macroscopic true strain (E_{cell}^{true}) is defined as illustrated in Fig. 7b. Combined with the discretization of the austenite volume fraction evolution, this procedure allows computing many unit cell responses ($\Sigma_{cell}-E_{cell}$) for different levels of deformation at which transformation initiates $E_{tsf}^{init,cell}$. These responses are next recombined using the averaging scheme described in Section 3.3.

3.3. Averaging scheme

After computing individual unit cell material responses ($\Sigma_{cell}-E_{cell}$) corresponding to different transformation initiation strains through relationship (1), they are recombined by means of a weighted sum of the unit cell calculations, in order to evaluate the global material behavior. An equal weighting factor ω_{cell} is imposed here on each unit cell based on

$$(\Sigma, E)_{Global} = \sum_{Cells} \omega_{cell} \times (\Sigma, E)_{Cell} = \frac{\sum_{Cells} (\Sigma, E)_{Cell}}{N} \quad (15)$$

where N is the total number of cells in the set of computations for a given transformation kinetics. As a result of the incorporation of a finite number of cell models by means of weighting factors, the global material response exhibits an oscillatory pattern with sudden drops corresponding to the transient response of each unit cell during a transformation event. As an example, a set of individual cell responses and their weighted sum corresponding to the transformation kinetics at $80\text{ }^{\circ}\text{C}$ is depicted in Fig. 8a and b, respectively. In order to remove these oscillations from the results, a cubic spline smoothing is then performed as illustrated in

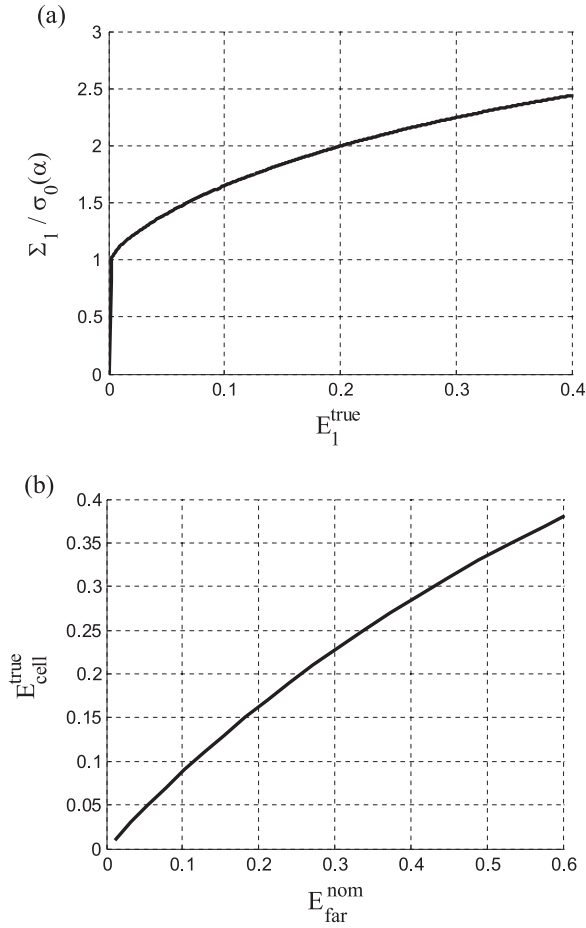


Fig. 7. Determination of the unit cell loading conditions: (a) average response of the non-transforming austenite-ferrite cell under far field uniaxial tensile loading with $l^*/D_{Aus}=3/4$, (b) link between true strain in the cell and the corresponding far field nominal strain.

Fig. 8c, see (MATLAB and Toolbox, 2013) for more details. Further post-processing analysis such as the detection of the onset of necking based on the Considère criterion, is extracted from the smoothed material response in the sequel.

4. Simulation of isothermal tensile tests

4.1. Material properties

A Swift type hardening law has been used in the sequel to represent the plastic flow of the different phases

$$\sigma_y = \sigma_0(1 + k E_p)^n \quad (16)$$

where σ_y and σ_0 are the current and initial yield stress, respectively, k is a hardening coefficient, while n is the strain hardening exponent. The hardening law parameters are evaluated based on generalized effective plastic strain E_p defined by Eq. (3). The material properties of the different phases are presented in Table 2. These parameters are based on an experimental elastic-plastic material characterization of a given type of TRIP assisted multiple-phase steel, Lacroix (2007). In order to limit the number of parameters to be identified, these properties are assumed temperature independent. The material properties of the region undergoing the transformation are taken as a linear interpolation between the properties of austenite and martensite over the course of transformation (stage 2 in Section 2.2). Furthermore, the material length parameter l_* , normalized by the diameter of the initial austenite inclusion l/D_{Aus} , will be varied from 0 (classical plasticity) to 1.25. A typical austenitic inclusion with a diameter of 2 μm is considered in this work. For this austenitic inclusion size, the range of values for l_* is centered around 1 μm , which is the usual value found for the present class of SGP theory, see e.g. Fleck and Hutchinson (2001); Evans and Hutchinson (2009); Massart and Pardoën (2010) and Brugger et al. (2010) for more details.

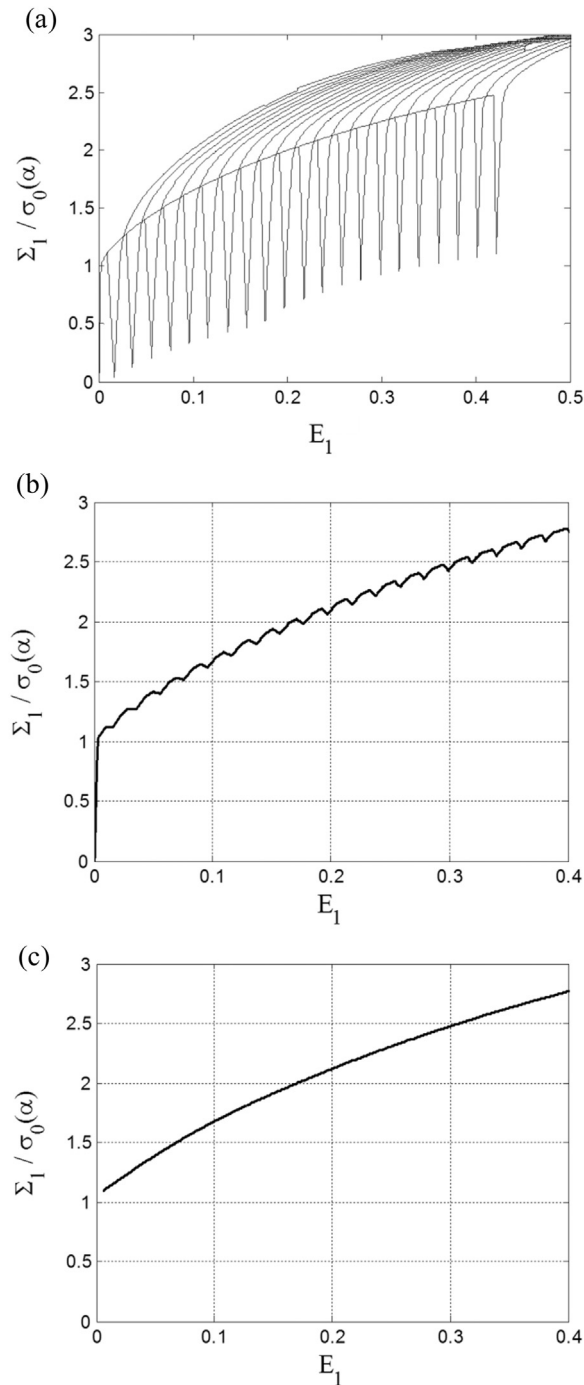


Fig. 8. Example of one application of the material behavior prediction by averaging many unit cell computations: (a) results of individual unit cells material response for the case $+80^\circ\text{C}$ with $l^*/D_{A_{111}}=0.75$ with increasing strain levels at the start of the transformation, (b) weighted sum of the individual unit cell curves, (c) fitted curve to the oscillating recombinant curves by means of cubic smoothing spline between 1% and 40% true strain.

4.2. Identification on the isothermal tensile tests

Based on the experimental transformation kinetics, depicted in Fig. 1, isothermal tensile tests with martensitic transformation kinetics corresponding to different temperatures are simulated using the procedure described in Sections 2 and 3. In order to perform the computations with a physically meaningful set of material parameters, the material properties given in Table 2 were adjusted to qualitatively reproduce the incremental strain hardening and the level of strain at the onset of necking for the $+80^\circ\text{C}$ condition. Note that no quantitative fitting on the stress-strain curve was attempted because of the

Table 2

The material properties of the phases in the simulated TRIP steel.

	Mart.	Aus.	Ferr.	HOM.
E (GPa)	187	187	200	200
ν	0.3	0.3	0.3	0.3
σ_0 (MPa)	2000	700	500	515
k	800	50	23	26
n	0.05	0.3	0.37	0.37

simplifying assumptions used in the model, i.e. the use of a finite number of cells to sample the transformation kinetics, the effect of the assumed properties for the surrounding medium, the simplified microstructural morphology and the absence of temperature dependency of the flow properties. These parameters are in the range of values used in earlier studies e.g. (Delannay et al., 2008). The internal length parameter was selected as the one allowing the best agreement with the experimental strain at the onset necking given in Fig. 1. The stress-strain response obtained for different l^*/D_{Aus} are reported in Fig. 9 for the +80 °C condition. The curves are presented up to the point at which the necking condition is attained in the simulations based on the Considère criterion. Several sets of material properties of the phases can be identified, each with a different internal length scale l^* to reproduce the overall curve at +80 °C. Among all these identified sets of parameters, the one reproducing at best the trend on the strain at the onset of necking attained at other temperatures was selected as the master set. Unless otherwise stated (in Section 6) the subsequent simulation results are obtained using this master set, including the intrinsic length scale D_{Aus} (with D_{Aus}). In subsequent figures, $l^*_0 = 0$ refers to the results obtained with a classical plasticity formulation which will be discussed later.

In Fig. 10a, the macroscopic tensile true stress (Σ) is plotted as a function of the macroscopic true strain (E) along the loading direction for isothermal tensile tests at –30 °C, +20 °C and +80 °C, respectively. These macroscopic stress-strain curves are normalized and are limited to the strain range prior to necking as detected based on the obtained stress-strain responses using Considère plots, see Fig. 10b. The different temperatures and corresponding transformation kinetics lead to a drop of true strain at the onset of necking from 0.38 for the test at +80 °C down to 0.27 at +20 °C and 0.21 at –30 °C. This drop agrees with the experimental trend, where the corresponding strains at the onset of necking are of 0.38 at +80 °C, 0.25 at +20 °C and 0.16 at –30 °C. It is noted that a perfect match is not obtained, mainly because of the above mentioned simplifying assumptions and the absence of temperature dependency in the hardening law of the ferrite phase. Even though no perfect fitting was attempted on the stress-strain curve for the same reasons, a substantial effect on the stress levels at lower temperatures is captured. These results show that the strain gradient plasticity formulation is an essential ingredient needed to capture the hardening rate. In particular, reproducing the trend with classical plasticity, using mean field theory approaches, requires an adjustment of the phase parameters to artificially generate a harder ferrite-based matrix close to the martensite region (Delannay et al., 2008). In order to further illustrate the need to use the SGP formulation, the same procedure was followed based on classical (non-size sensitive) J_2 plasticity to analyze the influence of the kinetics in a size independent plasticity framework. In Fig. 10, the material responses obtained using classical plasticity are presented with dashed lines. Fig. 10 proves that without SGP, the effect from the TRIP mechanism does not significantly modify the hardening rate. Without strain gradient plasticity effects, the results show that the material hardening rates in the different isothermal tensile tests are almost equivalent, with a much lower variation of the strain level at the onset of necking than in the experiments, ranging from 0.32 to 0.34 only. The responses for cases in which the grain is assumed to be either fully γ

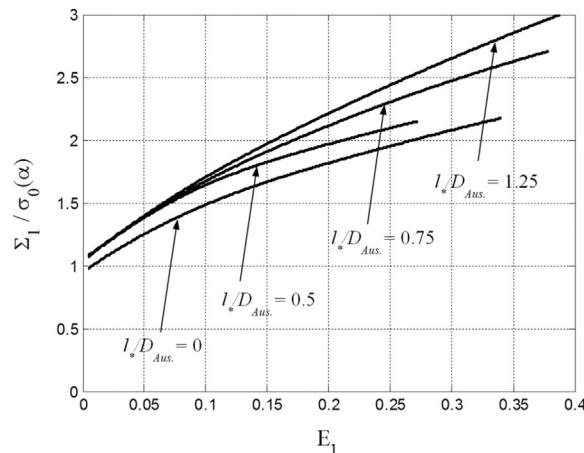


Fig. 9. Predicted material response (normalized by the yield stress of ferrite) corresponding to the isothermal tensile tests at +80 °C using the strain gradient plasticity formulation with different values of l^*/D_{Aus} ($l^*_0 = 0$ refers to the results obtained with classical plasticity without size effect).

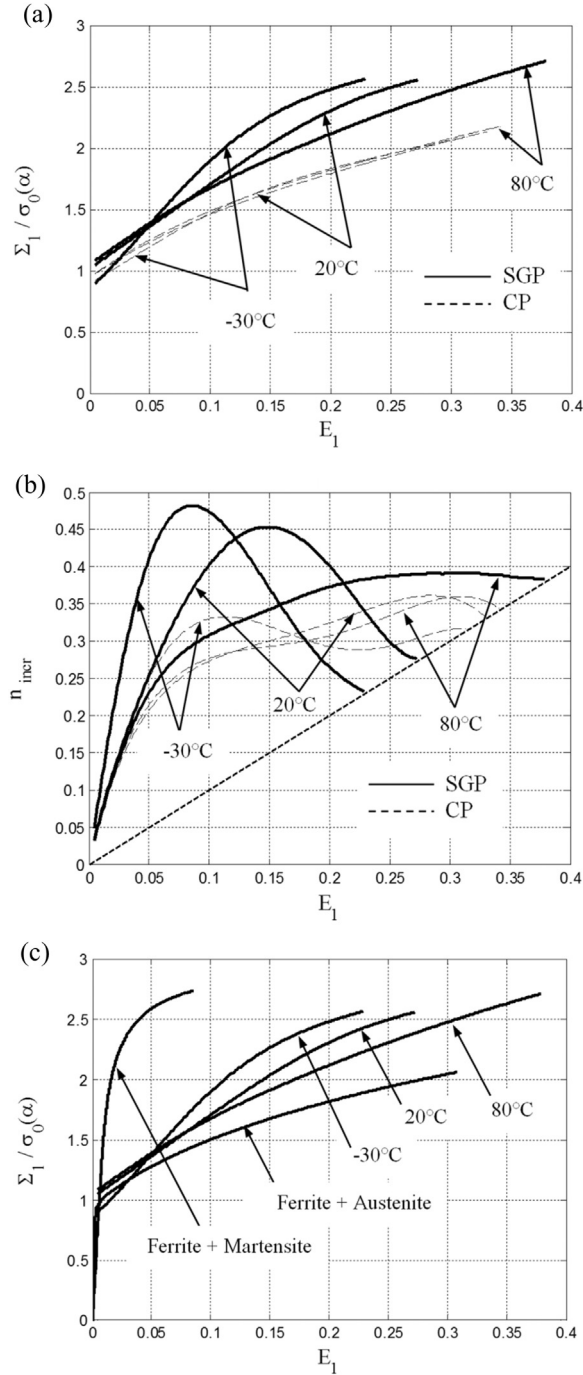


Fig. 10. Computational simulation of isothermal uniaxial tensile response using a classical plasticity formulation (dashed line) and the SGP formulation with $l^*/D_{AUS}=0.75$ at different temperatures corresponding to the austenite volume fraction evolution rate reported in Fig. 1. (a) True stress-strain curve, normalized with respect to the initial yield of the “ α ” phase, (b) corresponding Considère plot for the detection of the strain at the onset of necking; (c) extreme cases in which no transformation occurs, in one case the grain is assumed to be fully austenite while in the other one is fully martensite as from the loading initiation.

(i.e. no transformation, duplex steel) or fully α' (i.e. dual-phase steel) are shown in Fig. 10c, showing that all the results with a TRIP effect remain bounded by these two extreme cases in terms of strength levels. What is truly remarkable is that the TRIP steels outperform the full γ steel in terms of ductility at 80 °C.

As mentioned in Section 2.5, the selection of the properties of the surrounding medium as a (non-evolving) ferrite+austenite composite introduces an approximation for the unit cells with transformation at large deformation levels.

Such cells are in reality embedded in a medium with properties closer to the resulting TRIP steel behavior, that should be ideally obtained as an output of the averaging procedure. To avoid this approximation, the best approach would consist in recomputing new responses of the unit cells with a surrounding medium characterized by the curves depicted in Fig. 10a for each of the kinetics in a self-consistent manner. It would also require recomputing curves in Fig. 7b for these new surrounding properties. Recombining the unit cell responses obtained with these new surrounding properties would allow deducing a corrected set of results. The procedure should then be repeated until convergence of the results.

In order to check the impact of the surrounding medium properties on the predictions, a second round of unit cell computations was run using the stress-strain response from Fig. 10a for the surrounding properties. The main results regarding the strain at the onset of necking were unchanged, involving the strong variation of the strain at the onset of necking between the transformation kinetics associated with the three temperatures. Nevertheless, some moderate differences in the stress levels obtained at the different temperatures were found showing that a truly quantitative prediction of the experimental results would indeed require to systematize this more sophisticated self-consistent procedure.

5. Simulation of non-isothermal tensile test

Although it was shown in the previous section that a SGP model is absolutely necessary to capture the effect of the transformation kinetics on the TRIP response, additional comparison with experimental data can be used for further assessment. New experimental results involving sharp temperature changes in the course of the deformation are now addressed for this purpose. Two sets of experiments are therefore considered involving a first deformation at either $-30\text{ }^{\circ}\text{C}$ or $80\text{ }^{\circ}\text{C}$ followed by room temperature traction, referred as $-30/20$ and $80/20$ cases, accompanied with the measured transformation kinetics. The experimental responses are shown in Fig. 11a–c. The experimental kinetics in Fig. 11a is used as input for the simulations of $-30/20$ and $80/20$ conditions. According to Fig. 11, for the case “ $80/20$ ”, the transition occurs at a strain between 0.10 and 0.21, while in the case “ $-30/20$ ”, the transition starts at 0.025. Similar to the isothermal case, the numerical investigation is continued to a strain level larger than the onset of necking detected experimentally. The number of unit cells used in non-isothermal simulations is generally larger than in the isothermal cases in order to finely capture the transition between the kinetics associated with the initial and final temperatures. Finally, a similar procedure is applied to the combined curves to deduce the global material behavior. Fig. 12 presents the simulated material response for the “ $-30/20$ ” and “ $80/20$ ” cases, together with the corresponding Considère plots. The numerical results show that the case $-30/20$ has a higher hardening rate compared to the case $80/20$, in agreement with the corresponding experimental result. The macroscopic overall strain (E_1) at the onset of necking in the case “ $80/20$ ” is equal to 0.30, while it drops to 0.23 in the case “ $-30/20$ ”. This trend agrees with the experiments in which the strain at the onset of necking in the case “ $80/20$ ” is 0.08 larger than for the case “ $-30/20$ ”. Furthermore, a comparison between the iso- and non-isothermal analysis reveals that the onset of necking in the case “ $-30/20$ ” is delayed by only 0.015 compared to the isothermal case at $-30\text{ }^{\circ}\text{C}$. Conversely, necking occurs much earlier in the case “ $80/20$ ” in comparison with the isothermal case at $80\text{ }^{\circ}\text{C}$ (by 0.08 strain).

6. Towards transformation kinetics optimization

The objective is now to investigate additional fictitious transformation kinetics with a view on the strength/ductility balance optimization. For this purpose, the fictitious kinetics TK1, TK2 and OPTIM are considered as depicted in Fig. 13. TK1 represents a linear and extremely low rate of transformation, i.e. an additional isothermal case potentially matching a high temperature condition (higher than $+80\text{ }^{\circ}\text{C}$). On the other hand, TK2 represents a variable transformation rate which would be caused by successively increasing and decreasing the temperature during the tensile test around room temperature or by a distribution of two retained austenite families with different stabilities. Finally, the OPTIM kinetics assumes a low rate of transformation until a strain of 0.3 followed by a fast transformation in order to postpone necking.

In order to better understand the effect of l_* , the “fictitious” kinetics TK1 is used, focusing on the predicted onset of necking, see Fig. 14 for different values of l_*/D_{Aus} , ranging from 0 to 1.25. Once again, Fig. 14 shows that a classical plasticity model ($l_* = 0$) is not able to capture any evolution of the uniform elongation for different transformation kinetics. When considering the gradient plasticity based simulations, an effect of the transformation kinetics on the necking strain shows up for all isothermal cases. Fig. 14 shows that in the case of a fast transformation ($-30\text{ }^{\circ}\text{C}$ and $20\text{ }^{\circ}\text{C}$ kinetics), smaller sizes of the austenite grain (D_{Aus}) lead to smaller ductility. For the slow transformation ($80\text{ }^{\circ}\text{C}$ and TK1), there is a minimum ductility attained at an intermediate size, while, with a smaller microstructure size, the ductility keeps increasing with decreasing microstructural length. This is an important result which shows the high potential for improvement by microstructure refinement.

The fictitious kinetics denoted “OPTIM” involves an increase of the transformation kinetics at a strain of 0.3 in order to boost the strain hardening capacity when it is needed, i.e. near the Considère point. The results provided in Fig. 15 show that a very large ductility can be attained. These effects are further rationalized in Fig. 16 depicting the variation of the strain at the onset of necking as a function of an average rate of transformation combining all kinetics addressed in this study and the experimental data. This figure shows again that the experimental trend is very well captured. The OPTIM kinetics leads to a ductility that escapes from the general trend. Non monotonous transformation kinetics evolution appears thus to be very

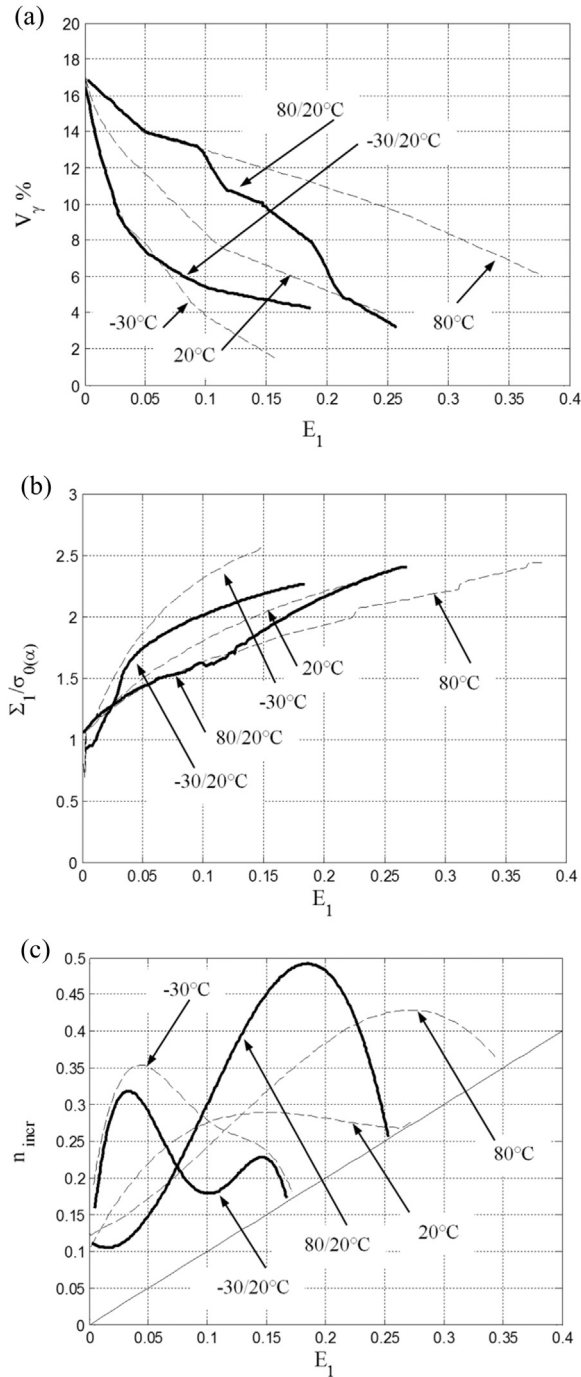


Fig. 11. Experimental results of non-isothermal uniaxial tensile tests with temperature variations bounded by the isothermal tests: (a) rate of austenitic volume fraction evolution, (b) true stress – true strain response, (c) considère plot for the determination of the strain at the onset of necking.

efficient to reach extreme ductility without loss of strength. The best performance can be attained with small microstructural sizes (to enhance the SGP effects) and a slow rate of transformation followed by an increased rate at large strains. From a metallurgical viewpoint this is certainly an interesting and meaningful option as the reduction of microstructure is usually accompanied by a slower transformation rate,² as for instance shown by Xiong et al. (2013) in the case of a new

² This also means that a fully predictive model involving a theoretical transformation law should involve, in the estimation of the mechanical driving force and accommodation terms, SGP effects in the formulation which goes far beyond the scope of this work.

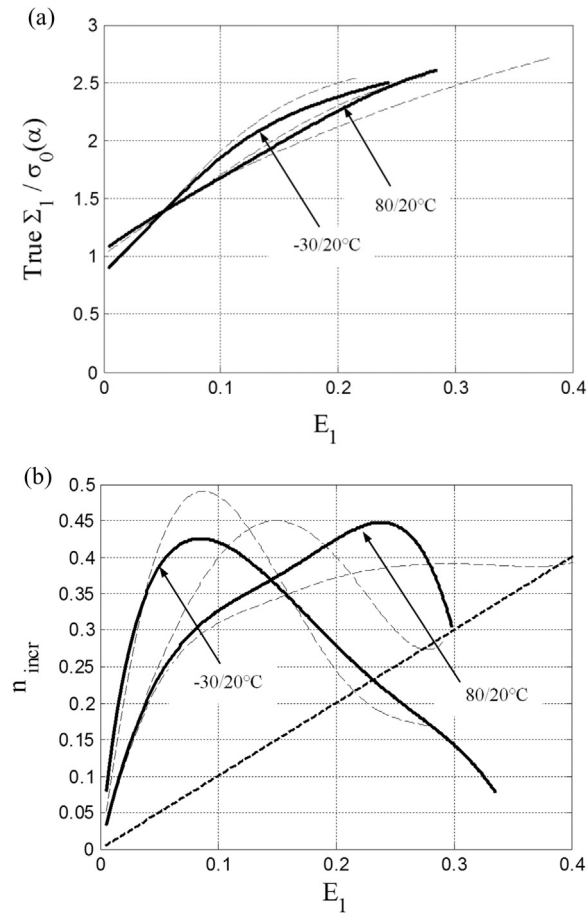


Fig. 12. Simulation of non-isothermal tensile tests with $I^*/D_{Aus.}=0.75$, at different temperature variations corresponding to the rate of evolution of the austenite volume fraction reported in Fig. 9. (a) true stress – true strain response, normalized with respect to the initial yield of the “ α ” phase, (b) Considère plot for the determination of the strain at the onset of necking.

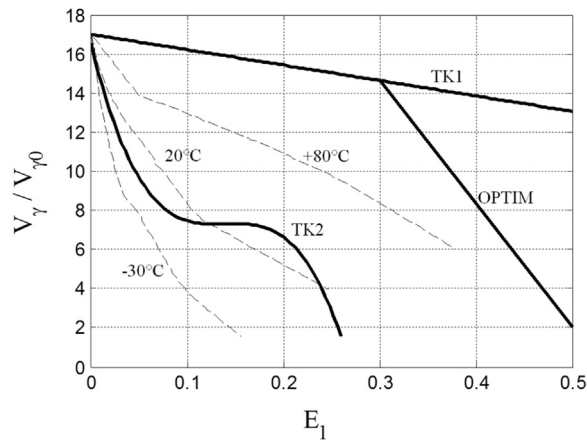


Fig. 13. Additional theoretical transformation kinetics.

generation of high strength steels.³ Hence, in 3rd generation high strength steels, the presence of retained austenite, which is already beneficial for ductility by allowing plastic flow between martensite laths (Maresca et al., 2014), can best contribute to strain hardening by TRIP effect if its size is very small (Raabe et al., 2009) and (Wang et al., 2014). Even though the

³ Note that Wang et al. (2014) have shown contradictory results in which smaller austenite layers are not necessarily more stable due to the occurrence of twinning when the size is sufficiently large.

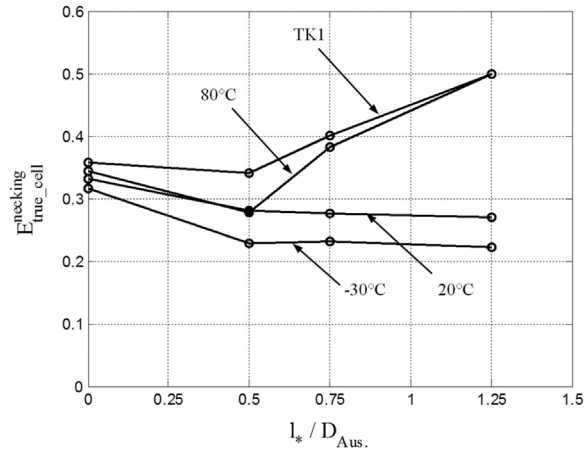


Fig. 14. (a) Variation of the volume fraction of retained austenite as a function of deformation for the isothermal experimental kinetics and the fictitious kinetics proposed to further analyze the TRIP effect (b) corresponding variation of the ductility as a function of the ratio $\frac{l^*}{D_{Aus.}}$ ($l^* = 0$ refers to the results obtained from classical plasticity formulation).

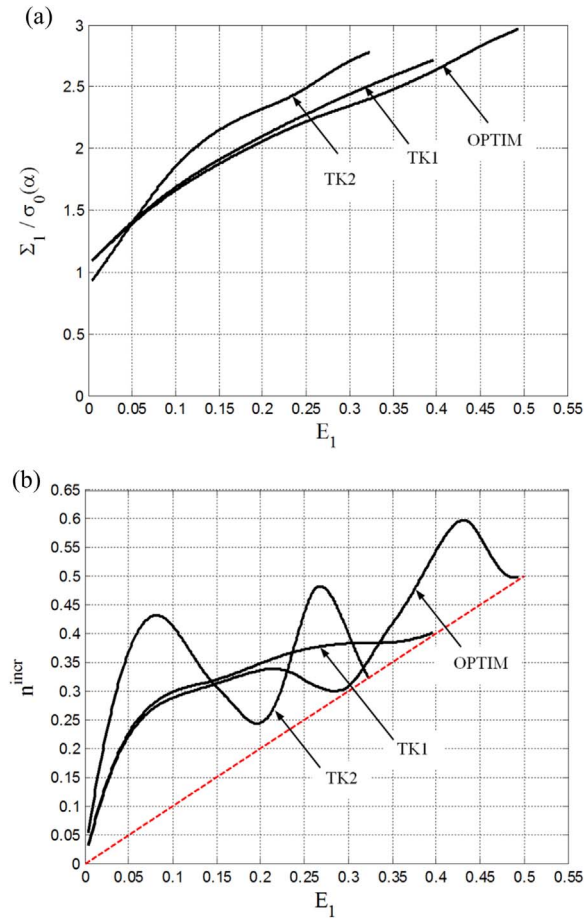


Fig. 15. Computational simulation of theoretical tensile tests with $l^*/D_{Aus.} = 0.75$, (a) true stress – true strain response, normalized with respect to the initial yield of the “ α ” phase, (b) considère plot for detection of the strain at the onset of necking.

behavior of interlath austenite involves several additional elements of complexity related to the dislocation/interface mechanisms and easy shear along the habit plane (Maresca et al., 2014), it can deliver a TRIP effect at moderate to large strains. One option to produce a transformation kinetics resembling OPTIM would be to combine both equiaxed retained austenite

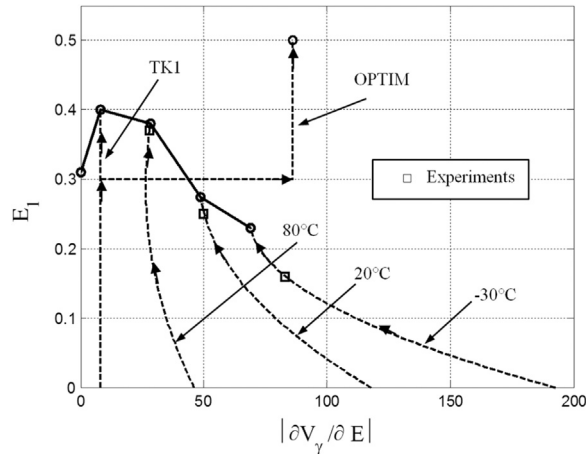


Fig. 16. Effect of the variation of the (practical and theoretically predicted) phase transformation kinetics on the onset of necking (necking with no transformation occurs at 0.32 true strain).

grains (with moderate transformation rates at intermediate strains) and sub-micron interlath austenite with delayed transformation in the same microstructure owing to proper heat treatments.

7. Conclusions

The macroscopic plastic response of TRIP assisted multiphase steels has been investigated, based on the homogenization of the behavior of elementary unit cells representing the microstructural local behavior of single austenite islands linked to the overall martensitic transformation kinetics. Size dependent plasticity was considered as key ingredient of the model suggested by many direct or indirect experiments or earlier modeling works. The [Fleck and Hutchinson \(2001\)](#) strain gradient plasticity theory has been used for this purpose within a finite strain setting.

The main conclusions of this study are the following:

- A comparison of the size dependent results with the trends obtained with a classical plasticity show that a size dependent framework is an essential feature in order to capture the effect of the transformation kinetics on the overall material behavior of TRIP assisted steels.
- For the identified set of material parameters, the computational results are in good agreement with the experiments in terms of the prediction of the ductility as a function of the transformation kinetics. This conclusion holds both for the isothermal and non-isothermal conditions, even using a rather simplified microstructural geometry representation. This is the first validation involving direct comparison with experimental data of the absolute need for a SGP type model to capture the TRIP effect in this class of steels.
- Parametric studies have been performed to investigate potential routes for further ductility optimization. A fictitious optimized kinetics assumes a transformation rate evolution able to provide strain hardening capacity when most needed in the deformation process. The combination of a refined microstructure with a transformation kinetics starting with a slow rate followed by a high rate at large strains results in a dramatic increase of the strain at the onset of necking.

Future works motivated by the present contribution should be focused on the means to generate practically refined microstructures, on the practical generation of microstructures exhibiting tailored transformation kinetics towards optimized ductility of TRIP assisted steels in the context of 3rd generation of high strength steels. From a modeling viewpoint, future works should investigate the possibility to incorporate more complex microstructural geometries ([Sonon et al., 2012](#)) and a SGP based transformation kinetics criterion.

Acknowledgments

This work was supported by Action de Recherche Concertée (ARC), Communauté française de Belgique, under Grant AUWB-2010-2015 ULB-No. 9. The first author acknowledges ULB for providing the financial support of Fonds Alice et David van Buren. The second and fifth authors were supported by the IAP project (Inter University Attraction Poles) P7/21 – Multiscale mechanics of interface dominated materials funded by BELSPO.

References

- Bhattacharyya, A., Weng, G., 1994. An energy criterion for the stress-induced martensitic transformation in a ductile system. *J. Mech. Phys. Solids* 42 (11), 1699–1724.
- Brugger, C., et al., 2010. Strain gradient plasticity analysis of the strength and ductility of thin metallic films using an enriched interface model. *Acta Mater.* 58 (15), 4940–4949.
- Cherkaoui, M., Berveiller, M., Sabar, H., 1998. Micromechanical modeling of martensitic transformation induced plasticity (TRIP) in austenitic single crystals. *Int. J. Plast.* 14 (7), 597–626.
- Delannay, L., Jacques, P.J., Pardoën, T., 2008. Modelling of the plastic flow of trip-aided multiphase steel based on an incremental mean-field approach. *Int. J. Solids Struct.* 45 (6), 1825–1843.
- Diani, J., Sabar, H., Berveiller, M., 1995. Micromechanical modelling of the transformation induced plasticity (TRIP) phenomenon in steels. *Int. J. Eng. Sci.* 33 (13), 1921–1934.
- Dong, M., Schmauder, S., 1996. Modeling of metal matrix composites by a self-consistent embedded cell model. *Acta Mater.* 44, 2465–2478.
- Evans, A.G., Hutchinson, J.W., 2009. A critical assessment of theories of strain gradient plasticity. *Acta Mater.* 57 (5), 1675–1688.
- Fischer, F., Oberaigner, E., Tanaka, K., Nishimura, F., 1998. Transformation induced plasticity revised an updated formulation. *Int. J. Solids Struct.* 35 (18), 2209–2227.
- Fleck, N.A., Hutchinson, J.W., 2001. A reformulation of strain gradient plasticity. *J. Mech. Phys. Solids* 49 (10), 2245–2271.
- Fleck, N.A., Muller, G., Ashby, M., Hutchinson, J.W., 1994. Strain gradient plasticity: theory and experiment. *Acta Metall. Mater.* 42 (2), 475–487.
- Geuzaine, C., Remacle, J.F., 2009. GMSH: A 3D finite element mesh generator with built-in pre- and post-processing facilities. *Int. J. Numer. Methods Eng.* 79 (11), 1309–1331.
- Godet, S., Jacques, P.J., 2015. Beneficial influence of an intercritically rolled recovered ferritic matrix on the mechanical properties of TRIP-assisted multiphase steels. *Mater. Sci. Eng.: A* 645, 20–27.
- Greenwood, G., Johnson, R., 1965. The deformation of metals under small stresses during phase transformations. *Proc. R. Soc. Lond. A: Math. Phys. Eng. Sci.* 283, 403–422.
- Hecker, S.S., Stout, M.G., Staudhammer, K.P., Smith, J.L., 1982. Effects of strain state and strain rate on deformation induced transformation in 304 stainless steel: Part I. magnetic measurements and mechanical behavior. *Metall. Trans. A* 13A, 619–626.
- Idesman, A.V., Levitas, V.I., Stein, E., 1999. Elastoplastic materials with martensitic phase transition and twinning at finite strains: numerical solution with the finite element method. *Comput. Methods Appl. Mech. Eng.* 173 (1), 71–98.
- Jacques, P.J., 2004. Transformation-induced plasticity for high strength formable steels. *Curr. Opin. Solid State Mater. Sci.* 8 (3), 259–265.
- Jacques, P.J., et al., 2007. Multiscale mechanics of TRIP-assisted multiphase steels: I. Characterization and mechanical testing. *Acta Mater.* 55 (11), 3681–3693.
- Jacques, P.J., Furnémont, Q., Pardoën, T., Delannay, F., 2001. On the role of martensitic transformation on damage and cracking resistance in TRIP-assisted multiphase steels. *Acta Mater.* 49 (1), 139–152.
- Kouznetsova, V., Geers, M.G.D., 2007. Modeling the interaction between plasticity and the austenite-martensite transformation. *Int. J. Multiscale Comput. Eng.* 5, 2.
- Lacroix, G., 2007. On the Relationships Between Microstructure and Mechanical Properties of TRIP-Assisted Multiphase Steels: Strength, Ductility, Fracture and Fatigue (Ph.D. dissertation). Université catholique de Louvain (UCL), Louvain-La-Neuve, Belgium.
- Lacroix, G., Pardoën, T., Jacques, P.J., 2008. The fracture toughness of TRIP-assisted multiphase steels. *Acta Mater.* 56 (15), 3900–3913.
- Lani, F., et al., 2007. Multiscale mechanics of TRIP-assisted multiphase steels: II. Micromechanical modelling. *Acta Mater.* 55 (11), 3695–3705.
- Leblond, J.-B., Mottet, G., Devaux, J., 1986. A theoretical and numerical approach to the plastic behaviour of steels during phase transformations—I. Derivation of general relations. *J. Mech. Phys. Solids* 34 (4), 395–409.
- Legartha, B.N., Niordson, C.F., 2010. Debonding failure and size effects in micro-reinforced composites. *Int. J. Plast.* 26, 149–165.
- Levitas, V., Idesman, A., Olson, G., 1998. Continuum modeling of strain-induced martensitic transformation at shear-band intersections. *Acta Mater.* 47 (1), 219–233.
- Magee, 1970. *Nucleation of martensite*. Phase Transformation, ASM, pp. 115–156.
- Maresca, F., Kouznetsova, V., Geers, M.G.D., 2014. Subgrain lath martensite mechanics: a numerical-experimental analysis. *J. Mech. Phys. Solids* 73, 69–83.
- Marketz, F., Fischer, F., 1994. Micromechanical modelling of stress-assisted martensitic transformation. *Model. Simul. Mater. Sci. Eng.* 2 (5), 1017.
- Marketz, F., Fischer, F., 1995. A mesoscale study on the thermodynamic effect of stress on martensitic transformation. *Metall. Mater. Trans. A* 26 (2), 267–278.
- Massart, T.J., Pardoën, T., 2010. Strain gradient plasticity analysis of the grain-size-dependent strength and ductility of polycrystals with evolving grain boundary confinement. *Acta Mater.* 58 (17), 5768–5781.
- MATLAB and Toolbox, S., 2013. Release 8.2.0.701 (R2013b). Natick, Massachusetts: The MathWorks Inc.
- Mazzoni-Leduc, L., Pardoën, T., Massart, T.J., 2008. Strain gradient plasticity analysis of transformation induced plasticity in multiphase steels. *Int. J. Solids Struct.* 45 (20), 5397–5418.
- Mazzoni-Leduc, L., Pardoën, T., Massart, T.J., 2010. Analysis of size effects associated to the transformation strain in TRIP steels with strain gradient plasticity. *Eur. J. Mech. – A/Solids* 29 (2), 132–142.
- Niordson, C.F., Hutchinson, J.W., 2003. Non-uniform plastic deformation of micron scale objects. *Int. J. Numer. Methods Eng.* 56 (7), 961–975.
- Niordson, C.F., Redanz, P., 2004. Size-effects in plane strain sheet-necking. *J. Mech. Phys. Solids* 52 (11), 2431–2454.
- Ognedal, A.S., et al., 2014. Void nucleation and growth in mineral-filled PVC – an experimental and numerical study. *Int. J. Solids Struct.* 51 (7), 1494–1506.
- Olson, G.B., Cohen, M., 1975. Kinetics of strain-induced martensitic nucleation. *Metall. Trans. A* 6 (4), 791–795.
- Olson, G.B., Azrin, M., 1978. Transformation behavior of TRIP steels. *Metall. Trans. A* 9A, 713–721.
- Pardoën, T., Massart, T.J., 2012. Interface controlled plastic flow modelled by strain gradient plasticity theory. *Comptes Rendus Méc.* 340, 247–260.
- Raabe, D., Ponge, D., Dmitrieva, O., Sander, B., 2009. Designing ultrahigh strength steels with good ductility by combining transformation induced plasticity and martensite aging. *Adv. Eng. Mater.* 11 (7), 547–555.
- Sonon, B., François, B., Massart, T.J., 2012. A unified level set based methodology for fast generation of complex microstructural multi-phase RVEs. *Comput. Methods Appl. Mech. Eng.* 223–224, 103–122.
- Srivastava, A., Ghassemi-Armaki, H., Sung, H., Chen, P., Kumar, S., Bower, A.F., 2015. Micromechanics of plastic deformation and phase transformation in a three-phase TRIP-assisted advanced high strength steel: experiments and modeling. *J. Mech. Phys. Solids* 78, 46–69.
- Stringfellow, R., Parks, D., Olson, G., 1992. A constitutive model for transformation plasticity accompanying strain-induced martensitic transformations in metastable austenitic steels. *Acta Metall. Mater.* 40 (7), 1703–1716.
- Tomita, Y., Iwamoto, T., 1995. Constitutive modeling of TRIP steel and its application to the improvement of mechanical properties. *Int. J. Mech. Sci.* 37 (12), 1295–1305.
- Turteltaub, S., Suiker, A., 2006a. A multiscale thermomechanical model for cubic to tetragonal martensitic phase transformations. *Int. J. Solids Struct.* 43 (14), 4509–4545.
- Turteltaub, S., Suiker, A., 2006b. Grain size effects in multiphase steels assisted by transformation-induced plasticity. *Int. J. Solids Struct.* 43 (24), 7322–7336.
- Van Rompaey, T., et al., 2006. Three-dimensional computational-cell modeling of the micromechanics of the martensitic transformation in transformation-induced-plasticity-assisted multiphase steels. *Metall. Mater. Trans. A* 37 (1), 99–107.
- Wang, M., et al., 2014. Smaller is less stable: size effects on twinning vs. transformation of reverted austenite in TRIP-maraging steels. *Acta Mater.* 79, 268–281.
- Xiong, X., et al., 2013. The effect of morphology on the stability of retained austenite in a quenched and partitioned steel. *Scr. Mater.* 68 (5), 321–324.
- Yen, H.-W., et al., 2015. Role of stress-assisted martensite in the design of strong ultrafine-grained duplex steels. *Acta Mater.* 82, 100–114.